A Divergence-Free Meshless Method Based on the Vector Basis Function for Transient Electromagnetic Analysis

Shunchuan Yang, *Student Member, IEEE*, Zhizhang Chen, *Fellow, IEEE*, Yiqiang Yu, *Member, IEEE*, and Sergey Ponomarenko

***Abstract*—Although meshless methods, in particularly those with scalar radial basis functions (RBFs), have been applied effectively to solve electromagnetic problems, their solutions may not be always divergence free in source-free regions, resulting in possibly large errors. In this paper, a new vector RBF based meshless method, which is divergence free, is proposed for solving transient electromagnetic problems. Its divergence properties are investigated and compared with those of scalar RBFs; and they are further verified with numerical examples that present good accuracy.**

***Index Terms*—Divergence free, meshless, transient analysis, vector radial basis function (RBF).**

I. Introduction

THE conventional numerical methods for solving electromagnetic problems, such as the finite-difference time-domain (FDTD) method [1], the finite-element method (FEM) [2] and the method of moments (MOM) [3], are grid- or cell-based techniques. For the FDTD method, discretization of solution domains can be considered as discretization with rectangles in two dimensions and cuboids in three dimensions [4]. For the FEM, continuous solution domains are usually discretized with triangles in two dimensions and tetrahedron in three dimensions [2]. These discretized cells are stacked together or inter-placed within each other and their interfaces then lead to grid or mesh lines whose intersections form spatial nodes. In other words, grid lines define spatial nodes associated with the finite cells and the connections among the nodes.

Manuscript received October 11, 2013; revised January 19, 2014 and April 24, 2014; accepted April 27, 2014. Date of publication May 14, 2014; date of current version July 01, 2014. The work of S. Yang was supported under Killam awards.

S. Yang and Z. Chen are with the School of Electronic Engineering, University of Electronic Science and Technology, Chengdu, Sichuan 610051, China, on leave from the Department of Electrical and Computer Engineering, Dalhousie University, Halifax, NS, Canada B3J 1Z1 (e-mail: sc.yang@dal.ca; z.chen@dal.ca).

Y. Yu is with the School of Information Engineering, East China Jiao Tong University, Nan Chang, Jiang Xi 330013, China, and also with the Department of Electrical and Computer Engineering, Dalhousie University, Halifax, NS, Canada B3J 1Z1.

S. Ponomarenko is with the Department of Electrical and Computer Engineering, Dalhousie University, Halifax, NS, Canada B3J 2X4.

Color versions of one or more of the figures in this paper are available online at http://ieeexplore.ieee.org.

Digital Object Identifier 10.1109/TMTT.2014.2322334

However, for practical structures with complex geometries, the above discretization scheme can become very complicated and even time consuming; in some situations, it may take the time longer than an actual field simulation time. In addition, when a small modification is made to a part of a structure to be solved, a re-discretization process may be needed for the whole solution domain due to repositioning of some grid lines than run through the whole solution domain. The time involved in re-discretization can be unacceptably long, especially for electrical large and multiscale structures.

To address the above issue, meshless methods are proposed where solution domains are discretized directly with spatial nodes instead of finite elements. They include the scalar radial basis function (RBF) method [5], the radial point interpolation method (RPIM) [6], the smoothed particle meshless method [7], and the edge-based smoothed point interpolation methods (PIMs) [8]. A 3-D RPIM was especially proposed in [9] and an unconditionally stable RPIM was presented in [10]. For most of these meshless methods, only spatial node information is needed to formulate electromagnetic problems. No connection information or grid lines among nodes are required. As a result, no rearrangements of grid lines are required when a structure is modified partially. In addition, [11] demonstrates the existence of spurious modes in the traditional RPIM.

In a continuous domain, electromagnetic fields observe the divergence property: magnetic fields are always divergence free and so are electrical fields in charge-free regions. When numerical methods are developed for solving electromagnetic problems, this divergence property may not be preserved numerically and spurious numerical solutions may emerge [12]. Indeed, it has been found that the original meshless method does not always have this divergence-free property; spurious solutions exist in the solutions obtained.

On the other hand, divergence-free RBFs were developed for nonelectromagnetic applications. A matrix-valued RBF, which is termed as the vector RBF in difference from the scalar RBF, was proposed and proven theoretically divergence free [13]. More work along this line was presented in [13]–[15]. In particular, the divergence-free vector RBF was successfully applied to the Navier–Stokes equation [15] and astrophysical magneto-hydrodynamics (MHD) [16]. However, to the best knowledge of the authors, no reports were seen to apply the vector RBFs to computational electromagnetics and little has been addressed on

divergence properties of numerical methods that solve electromagnetic problems.

In this paper, we propose a meshless method incorporated with the above vector RBF for transient electromagnetic analysis. The proposed meshless method is theoretically proven to be divergence free in the source-free region. Therefore, no artificial charges or spurious solutions will be present in the solutions of the meshless methods, making them more accurate.

This paper is organized in the following manner. In Section II, the traditional RBF meshless method is briefly introduced. In Section III, basics of the vector RBFs are presented and the properties of the scalar and vector RBFs are discussed. In Section IV, the formulations of the divergence-free meshless method for modeling electromagnetic fields are developed. In Section V, accuracy and divergence properties of the proposed meshless method are verified numerically. Finally, conclusions are drawn in Section VI.

II. Original Scalar RBF Meshless Method

In order to better understand the vector RBFs, we first give a brief introduction to the conventional scalar RBF meshless method in this section.

The scalar RBF method was firstly introduced to solve partial differential equations by Kansa [17], [18]. Consider an unknown function $f(\mathbf{R})$ that is interpolated with the function values at the discretized scattering points of x_i in a solution domain. $f(\mathbf{R})$ can then be approximated by the RBF as follows:

$$f(\mathbf{x}) = \sum_{j=1}^{N} \phi\left(\|\mathbf{R}-\mathbf{R}_j\|\right) a_j \tag{1}$$

where $\phi(\|\mathbf{R}-\mathbf{R}_j\|)$ is the RBF, $\mathbf{R}=(x,y,z)$ is the location of the point of interest, $\mathbf{R}_j=(x_j,y_j,z_j)$ is the location of node j, N is the number of nodes in a local support domain, and a_i are the unknown expansion coefficients. Several different types of RBFs can be used in (1). We select the Gaussian function as the scalar RBF in this paper. Its formulation can be expressed as

$$\phi_j = \phi\left(\|\mathbf{R}-\mathbf{R}_j\|\right) = e^{-\alpha r^2} \tag{2}$$

where $r = \|\mathbf{R}-\mathbf{R}_j\|$ is the Euclidean distance between the point of interest and node j, and α is the shape parameter that controls the decaying rate of the basis function.

To find the unknown expansion coefficients, (1) is enforced to pass through all the nodes within a local support domain. A set of linear equations corresponding to the nodes is then obtained and it can be rewritten in the following compact matrix form:

$$\mathbf{A}\cdot\mathbf{a} = \mathbf{f} \tag{3}$$

where $f_s = [f_1\ f_2\ \cdots\ f_N]^T$ with f_i being the value of function f at node i. $a = [a_1\ a_2\ \cdots\ a_N]^T$ and

$$\mathbf{A} = \begin{bmatrix} \phi(\|\mathbf{R}_1-\mathbf{R}_1\|) & \phi(\|\mathbf{R}_1-\mathbf{R}_2\|) & \cdots & \phi(\|\mathbf{R}_1-\mathbf{R}_N\|) \\ \phi(\|\mathbf{R}_2-\mathbf{R}_1\|) & \phi(\|\mathbf{R}_2-\mathbf{R}_2\|) & \cdots & \phi(\|\mathbf{R}_2-\mathbf{R}_N\|) \\ \vdots & \vdots & & \vdots \\ \phi(\|\mathbf{R}_N-\mathbf{R}_1\|) & \phi(\|\mathbf{R}_N-\mathbf{R}_2\|) & \cdots & \phi(\|\mathbf{R}_N-\mathbf{R}_N\|) \end{bmatrix}. \tag{4}$$

Since $\mathbf{A}$ is always invertible (as (2) is selected as the RBF [20]), expansion coefficients a_i can be obtained by inverting $\mathbf{A}$. Substitution of a_i into (1) leads to

$$f = \mathbf{B}\mathbf{A}^{-1}\mathbf{f}_s = \mathbf{\Phi}\mathbf{f}_s \tag{5}$$

where $\mathbf{B} = \mathbf{B}(\|\mathbf{R}-\mathbf{R}_j\|)$ contains the RBFs, $\mathbf{\Phi} = [\Phi_1\ \Phi_2\ \cdots\ \Phi_N] = \mathbf{B}\mathbf{A}^{-1}$ and $\Phi_i = \Phi_i(\|\mathbf{R}-\mathbf{R}_j\|)$ is the shape function associated with spatial node i $(i=1,2,\ldots,N)$.

Since the shape function is a continuous function, its first-order partial derivatives can be analytically obtained as

$$\frac{\partial\mathbf{\Phi}}{\partial\kappa} = \frac{\partial\mathbf{B}\left(\|\mathbf{R}-\mathbf{R}_i\|\right)}{\partial\kappa}\mathbf{A}^{-1}. \tag{6}$$

III. Proposed Vector RBF Meshless Method

In this section, we propose the divergence-preserved meshless method with the vector RBFs presented in [13]–[15] and then analytically prove the divergence properties of the method. We also examine other properties of the method.

A. Proposed Vector-Based RBF

Mathematically, a divergence-free field, denoted as $\mathbf{u}$, can always be expressed as the curl of another vector field, say, $\mathbf{w}$, as follows:

$$\mathbf{u} = \nabla\times\mathbf{w} \tag{7}$$

where $\nabla = [\partial/\partial x, \partial/\partial y, \partial/\partial z]^T$.

$\mathbf{w}$ is not unique in (7). Therefore, additional conditions are needed. One common choice is Coulomb gauge, $\nabla\bullet\mathbf{w}=0$, which means that we can let $\mathbf{w}$ be the curl of a third vector function. In our case, we select the following form:

$$\mathbf{w}(\mathbf{x}) = \nabla\times\sum_{j=1}^{N}\phi(\mathbf{R}-\mathbf{R_j})\mathbf{A}_j \tag{8}$$

where ϕ is a preselected scalar basis function and $\mathbf{A}_j = (A_{xj}, A_{yj}, A_{zj})^T$ is the unknown vector expansion coefficient to be determined. Equation (8) forms the basis function expansion of the vector field $\mathbf{u}$, and consequently, vector field $\mathbf{u}$ can be expressed as

$$\begin{aligned}\mathbf{u} &= \nabla\times\nabla\times\sum_{j=1}^{N}\phi(\mathbf{R}-\mathbf{R_j})\mathbf{A}_j \\ &= (-\Delta\mathbf{I}+\nabla\nabla^T)\sum_{j=1}^{N}\phi(\mathbf{R}-\mathbf{R_j})\mathbf{A}_j\end{aligned} \tag{9}$$

where $\mathbf{I}$ is the 3×3 identity matrix, and Δ is the Laplace operator, which can be expressed as

$$\Delta = \begin{bmatrix} \frac{\partial^2}{\partial x^2}+\frac{\partial^2}{\partial y^2}+\frac{\partial^2}{\partial z^2} & & \\ & \frac{\partial^2}{\partial x^2}+\frac{\partial^2}{\partial y^2}+\frac{\partial^2}{\partial z^2} & \\ & & \frac{\partial^2}{\partial x^2}+\frac{\partial^2}{\partial y^2}+\frac{\partial^2}{\partial z^2} \end{bmatrix}. \tag{10}$$

Based on (9), we can then define the vector RBF $\mathbf{\Psi}_j$ related to node j and shape function $\mathbf{\Phi}$ as

$$\mathbf{\Psi}_j = (-\Delta \mathbf{I} + \nabla\nabla^T)\phi_j \tag{11a}$$

$$\mathbf{\Phi} = \mathbf{B}_v \mathbf{A}_v^{-1} \mathbf{u}_s \tag{11b}$$

and

$$\mathbf{u} = \sum_{j=1}^{N} \mathbf{\Phi}_j \mathbf{u}_j \tag{11c}$$

where $\mathbf{B}_v$ contains the vector RBFs, $\mathbf{u}_s = [\dots\ u_{jx}\ u_{jy}\ u_{jz}\ \cdots]^T$, $\mathbf{u}_j = [u_{jx}\ u_{jy}\ u_{jz}]^T$, and

$$\mathbf{A}_v = \begin{bmatrix} \mathbf{\Psi}(\|\mathbf{R}_1-\mathbf{R}_1\|) & \mathbf{\Psi}(\|\mathbf{R}_1-\mathbf{R}_2\|) & \cdots & \mathbf{\Psi}(\|\mathbf{R}_1-\mathbf{R}_N\|) \\ \mathbf{\Psi}(\|\mathbf{R}_2-\mathbf{R}_1\|) & \mathbf{\Psi}(\|\mathbf{R}_2-\mathbf{R}_2\|) & \cdots & \mathbf{\Psi}(\|\mathbf{R}_2-\mathbf{R}_N\|) \\ \vdots & \vdots & & \vdots \\ \mathbf{\Psi}(\|\mathbf{R}_N-\mathbf{R}_1\|) & \mathbf{\Psi}(\|\mathbf{R}_N-\mathbf{R}_2\|) & \cdots & \mathbf{\Psi}(\|\mathbf{R}_N-\mathbf{R}_N\|) \end{bmatrix}.$$

The dimension of $\mathbf{A}_v$ is $3N \times 3N$, where N is the number of scattering nodes in a local support domain. Since the number of nodes, N, in a local support domain is small, inversion of $\mathbf{A}_v$ can be done without much difficulty with modern computers.

Several observations can be made on the vector basis function of (11) as follows.

1) The vector basis function can be constructed from the scalar RBF,ϕ_j, with a 3×3 matrix transform for each node j through (11a).
2) ϕ_j can be any kind of basis function including RBF or Gaussian function.
3) The shape function $\mathbf{\Phi}_j$ satisfies Kronecker's delta property, i.e.,

$$\mathbf{\Phi}_j = \begin{cases} \mathbf{I}, & \mathbf{R} = \mathbf{R}_j \\ \mathbf{0}, & \text{at other nodes.} \end{cases} \tag{12}$$

4) Each row of $\mathbf{\Psi}_j$ is a vectorized basis function: the first row of $\mathbf{\Psi}_j$, or the first vector in the vector RBF, represents the x component, the second vector (row) the y component, and the third vector the z component, respectively.

Expansion of (11) for each node reads

$$\mathbf{\Psi}_j = \begin{bmatrix} -\partial_y^2 - \partial_z^2 & \partial_x\partial_y & \partial_x\partial_z \\ \partial_y\partial_x & -\partial_x^2 - \partial_z^2 & \partial_y\partial_z \\ \partial_z\partial_x & \partial_z\partial_y & -\partial_x^2 - \partial_y^2 \end{bmatrix} \phi_j. \tag{13}$$

The curl of $\mathbf{\Psi}_j$ can be found as shown in (14) at the bottom of this page.

For a 2-D problem, fields are assumed constant in the z-direction; therefore, $\partial_z = 0$. The vector RBFs and their curl operation are much simplified. More specifically, we have

$$\mathbf{\Psi}_j = \begin{bmatrix} -\partial_y^2 & \partial_x\partial_y & 0 \\ \partial_x\partial_y & -\partial_x^2 & 0 \\ 0 & 0 & -\partial_y^2 - \partial_x^2 \end{bmatrix} \phi_j \tag{15}$$

and

$$\nabla \times \mathbf{\Psi}_j = \begin{bmatrix} 0 & 0 & \partial_x^2\partial_y + \partial_y^3 \\ 0 & 0 & -\partial_y^2\partial_x - \partial_x^3 \\ -\partial_x^2\partial_y - \partial_y^3 & \partial_y^2\partial_x + \partial_x^3 & 0 \end{bmatrix} \phi. \tag{16}$$

Here the scalar RBF is chosen to be $\phi_j = (1/2\alpha)e^{-\alpha[(x-x_j)^2+(y-y_j)^2]}$, which results in

$$\Psi_{j11} = \left[2\alpha(x-x_j)^2 - 1\right] e^{-\alpha\left[(x-x_j)^2+(y-y_j)^2\right]} \tag{17a}$$

$$\Psi_{j12} = 2\alpha(x-x_j)(y-y_j) e^{-\alpha\left[(x-x_j)^2+(y-y_j)^2\right]} \tag{17b}$$

$$\Psi_{j21} = \Psi_{j12} \tag{17c}$$

$$\Psi_{j22} = \left[2\alpha(y-y_j)^2 - 1\right] e^{-\alpha\left[(x-x_j)^2+(y-y_j)^2\right]} \tag{17d}$$

$$\Psi_{j33} = \left[2\alpha(x-x_j)^2 + 2\alpha(y-y_j)^2 - 2\right] \times e^{-\alpha\left[(x-x_j)^2+(y-y_j)^2\right]}. \tag{17e}$$

To better understand the vector basis function, we plot a 2-D vector RBF at $\boldsymbol{R}_j = [0\ 0]^T$ using (2) as the scalar basis function with $\alpha = 5$ [16]. Fig. 1 shows the vector RBF in the two dimensions. The first vector is the first row of (15) and the second vector is the second row of (15). It is easy to see that the two rows of the vector RBF present two mutually orthogonal dipole modes: Fig. 1(a) is the horizontal dipole mode and Fig. 1(b) is the vertical dipole mode; rotation of one dipole leads to another. Obviously, both dipole modes are divergence free. Thus, the field expanded by them should be divergence free.

B. Divergence of the Proposed Vector RBF

Since $\mathbf{\Psi}$ is constructed from (7) and (8), its divergence should be zero as implied by (8). We can verify it by directly taking the divergence of the mth row of $\mathbf{\Psi}$,

$$\begin{aligned} \nabla \bullet (\mathbf{\Psi}_j)_m &= \nabla \bullet \left\{(-\Delta \mathbf{I} + \nabla\nabla^T)\phi_j\right\}_m \\ &= \nabla \bullet \left\{-\delta_{mn} \sum_{p=x,y,z} \frac{\partial^2}{\partial p^2} + \frac{\partial}{\partial k}\frac{\partial}{\partial l}\right\} \phi_j \\ &= \left\{-\sum_{p=x,y,z} \frac{\partial^2}{\partial p^2}\frac{\partial}{\partial k} + \sum_{p=x,y,z} \frac{\partial^2}{\partial p^2}\frac{\partial}{\partial k}\right\} \phi_j \\ &= 0 \end{aligned} \tag{18}$$

where k and l stand for the other two directions in a Cartesian coordinate system rather than p, and m and n represents the mth row and nth column of $\mathbf{\Psi}_j$.

$$\nabla \times \mathbf{\Psi}_j = \begin{bmatrix} 0 & -\partial_x^2\partial_z - \partial_z^3 - \partial_y^2\partial_z & \partial_x^2\partial_y + \partial_y^3 + \partial_z^2\partial_y \\ \partial_x^2\partial_z + \partial_z^3 + \partial_y^2\partial_z & 0 & -\partial_z^2\partial_x - \partial_x^3 - \partial_y^2\partial_x \\ -\partial_x^2\partial_y - \partial_y^3 - \partial_z^2\partial_y & \partial_z^2\partial_x + \partial_x^3 + \partial_y^2\partial_x & 0 \end{bmatrix} \phi_j \tag{14}$$

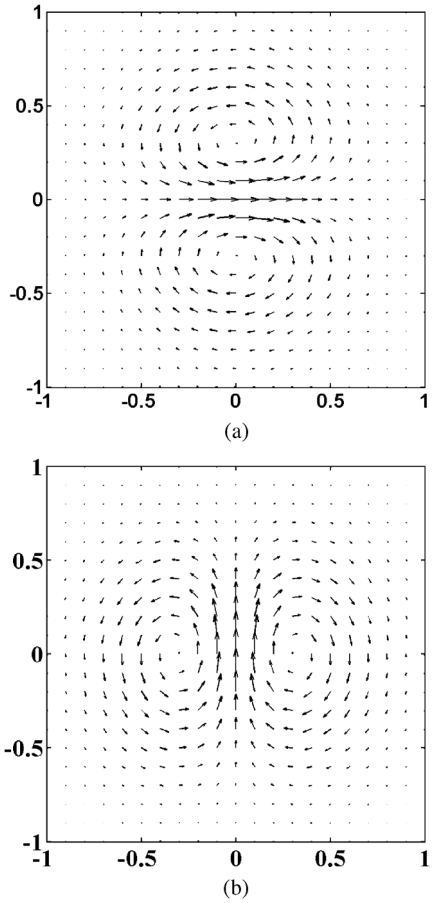

Fig. 1. Plots of the vector RBF modes with $\alpha = 5$. (a) First vector. (b) Second vector.

C. Divergence Properties of the Scalar RBF

In this section, we examine the divergence properties of the original meshless method that uses the scalar RBF. As shown in Section II, the field in the conventional mesheless method is approximated as

$$u = \sum_{j=1}^{N} \phi_j \alpha_j = \sum_{j=1}^{N} \phi(\mathbf{R} - \mathbf{R_j})\alpha_j \tag{19}$$

at each node. Assume that the Gaussian function of (2) is used as the basis function ϕ. The divergence of the approximated field (19) can then be found as

$$\nabla \bullet \mathbf{u} = -2\alpha e^{-\alpha r^2} \sum_{j=1}^{N} (x + y + z - x_j - y_j - z_j)a_j. \tag{20}$$

It is seen from (20) that the divergence of $\mathbf{u}$ is dependent on the position of the point of interest, the nodes, and the expansion coefficients. There is no guarantee that it will always be zero, except for the certain point of interest and node distributions that make (20) zero. In other words, the divergence-free property is not warranted for the scalar RBF meshless method. This is not the case for the proposed vector RBFs since they are constructed through (8), which ensures the divergence property.

IV. Proposed Meshless Formulations With the Vector RBF for Solving Electromagnetic Problems

A. Meshless Formulations

With the definition of the vector basis function and vector shape function, electrical and magnetic vector field can be approximated as

$$\mathbf{E} = \sum_{i}^{NA} \mathbf{\Phi}_i \mathbf{E}_i \tag{21a}$$

$$\mathbf{H} = \sum_{i}^{NB} \mathbf{\Phi}_i \mathbf{H}_i. \tag{21b}$$

Consider Maxwell's equations in a linear, isotropic, nondispersive, and lossless media/medium of permittivity ε and permeability μ without sources,

$$\frac{\partial \mathbf{H}}{\partial t} = -\frac{1}{\mu}\nabla \times \mathbf{E} \tag{22a}$$

$$\frac{\partial \mathbf{E}}{\partial t} = \frac{1}{\varepsilon}\nabla \times \mathbf{H}. \tag{22b}$$

By substitution of (21) into (22), we have the following equations:

$$\frac{\partial \sum_{i}^{NB} \mathbf{\Phi}_i \mathbf{H}_i}{\partial t} = -\frac{1}{\mu}\nabla \times \sum_{j}^{NA} \mathbf{\Phi}_j \mathbf{E}_j \tag{23a}$$

$$\frac{\partial \sum_{i}^{NA} \mathbf{\Phi}_i \mathbf{E}_i}{\partial t} = \frac{1}{\varepsilon}\nabla \times \sum_{j}^{NB} \mathbf{\Phi}_j \mathbf{H}_j. \tag{23b}$$

Now we choose the collocation method and apply it to the above equation, i.e., we choose a Dirac Delta function for the error testing or minimization [4]: test (23a) with Delta functions at magnetic field nodes, and (23b), with Delta functions at electric field nodes. Due to the Kronecker's Delta property of the vector shape function, we can then obtain the following equations:

$$\frac{\partial \mathbf{H_i}}{\partial t} = -\frac{1}{\mu}\nabla \times \sum_{j}^{NA} \mathbf{\Phi}_j \mathbf{E_j} \tag{24a}$$

$$\frac{\partial \mathbf{E_i}}{\partial t} = \frac{1}{\varepsilon}\nabla \times \sum_{j}^{NB} \mathbf{\Phi}_j \mathbf{H_j}. \tag{24b}$$

When the central finite-difference scheme is applied to (24) in time, the time-marching equation can be obtained,

$$\mathbf{H}_i^{n+1/2} = \mathbf{H}_i^{n-1/2} - \frac{\Delta t}{\mu} \sum_{j}^{NA} \nabla \times \mathbf{\Phi}_j \mathbf{E}_j^n \tag{25a}$$

$$\mathbf{E}_i^{n+1} = \mathbf{E}_i^n + \frac{\Delta t}{\varepsilon} \sum_{j}^{NB} \nabla \times \mathbf{\Phi}_j \mathbf{H}_j^{n+1/2}. \tag{25b}$$

Note that the shape functions in the above equations are naturally divergence free.

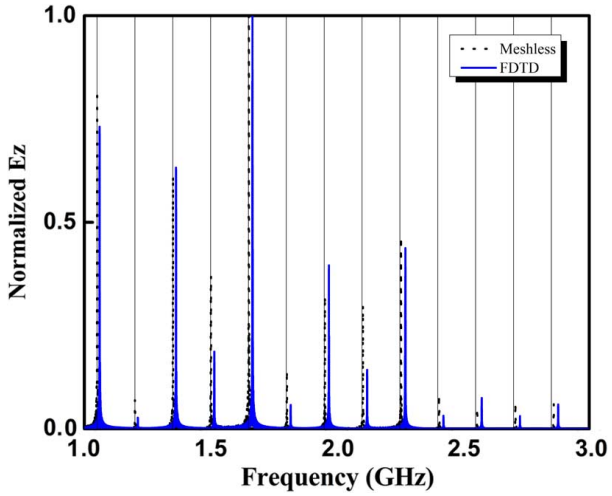

Fig. 2. Resonance frequencies obtained with the proposed meshless method and the FDTD method. The vertical grey lines represent the analytical resonant frequencies.

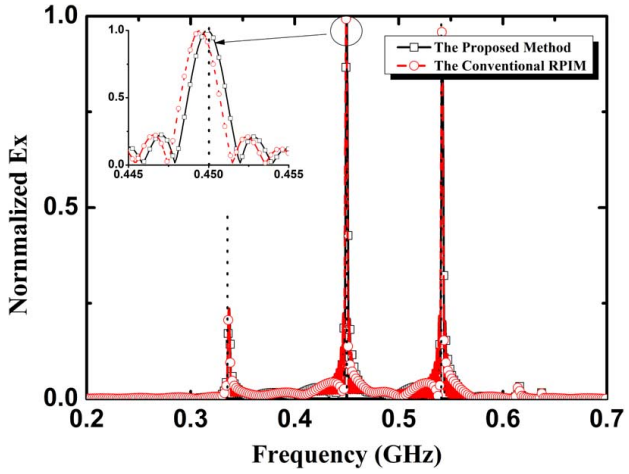

Fig. 3. Resonance frequencies obtained with the proposed meshless method and the conventional RPIM. The vertical grey lines represent the analytical resonant frequencies.

V. Numerical Examples and Discussion

In this section, a few numerical examples are presented to verify the divergence properties and accuracy of the proposed vector RBF based divergence-free meshless method. They are elaborated below.

A. 1-D Resonator

A 1-D resonator with perfect electrical conductor (PEC) walls at both ends was constructed. The length of the 1-D cavity is 1 m. The current source is located at the center and is specified as

$$J_z = \cos(2\pi f t) \exp\left(-\left(\frac{t_c - t}{t_w}\right)^2\right) \tag{26}$$

where $f = 1.5$ GHz, $t_w = 40$ ns, and $t_c = 120$ ns.

Fig. 2 shows the resonator frequencies obtained with the proposed meshless method and FDTD method. Both the uniform grid size for the FDTD method and the uniform node distance for the meshless method are 0.01 m; it amounts to ten cells or ten spatial sampling points per wavelength at 3 GHz across the whole computation domain. The theoretical resonance frequencies are represented with the vertical lines in the figure. It can be seen that the results obtained with the FDTD method have frequency shift towards a higher frequency region even when ten cells per wavelength is used at 3 GHz. However, the frequencies obtained with the proposed meshless method agree well with the theoretical results. In other words, the proposed meshless method has better accuracy than the FDTD method under the same discretization conditions. This may be attributed to the fact that the meshless method is essentially a high-order method while the FDTD method expands the field quantity with the rooftop function [4].

B. Cavity Without and With a Fin

A 2-D cavity with dimensions of 100 cm $\times$ 100 cm is considered. A uniform node distance is taken to be 5 cm. Fig. 3 shows the resonance frequencies obtained from the conventional RPIM and the proposed meshless method. The vertical dot lines indicate the theoretical results. Although the same node distribution was employed with the RPIM and the proposed meshless method, a small frequency difference from the theoretical results is observed at 0.45 GHz with the results obtained with the conventional RPIM. For the proposed meshless method, the results agree well with the theoretical results.

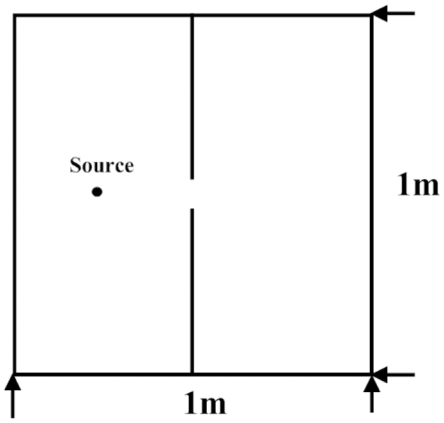

Fig. 4. Geometry of the cavity with PEC screen located at the middle.

To verify the divergence properties of the proposed meshless method based on the vector RBFs, we considered an air-filled finned cavity with the dimensions of 100 cm $\times$ 100 cm, as shown in Fig. 4. It was then discretized with a uniform grid of 20 cells $\times$ 20 cells and the cell size is 5 cm. Such a discretization arrangement amounts to 15 sampling points per wavelength at 0.4 GHz. The reason we chose the finned structure is that there should be strong charge accumulation at the edges of the fins and no charges is accumulated elsewhere. We can then evaluate the divergence property of the numerical methods in an effective way.

A point source of Gaussian pulse as follows was excited inside the cavity:

$$J_x = \cos(2\pi f t) \exp\left(-\left(\frac{t_c - t}{t_w}\right)^2\right) \tag{27}$$

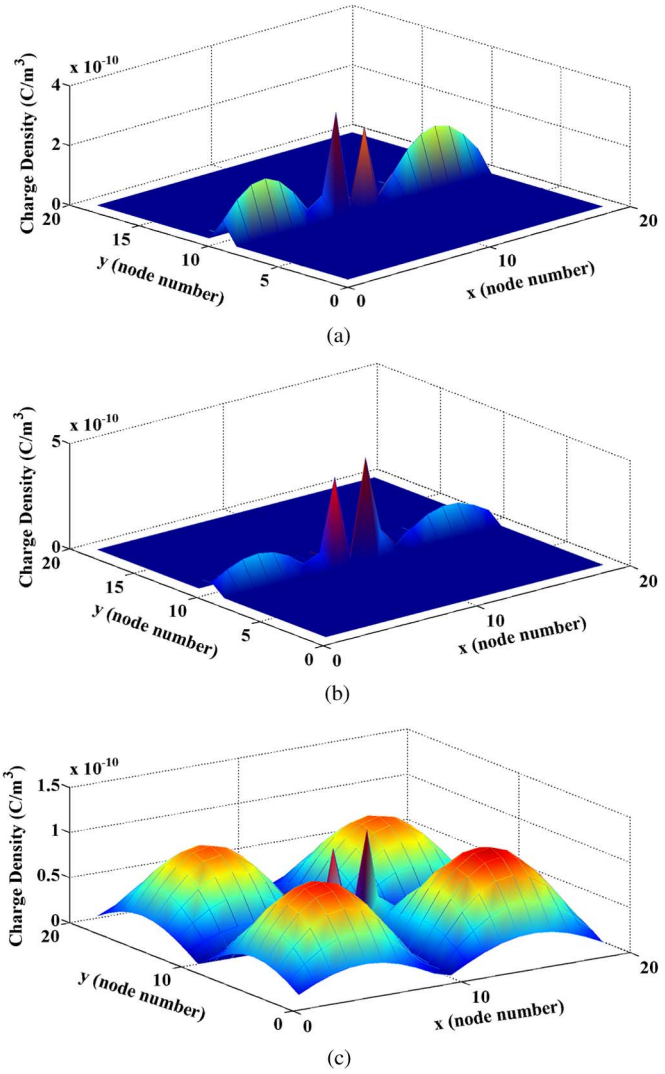

Fig. 5. (a) Charge density distribution obtained with the conventional FDTD method, (b) proposed meshless method based on vector RBFs, and (c) conventional meshless method based on the scalar RBFs at time $t = 50$ ns.

where $f = 0.4$ GHz, $t_w = 4$ ns, and $t_c = 12$ ns. The divergence of electric flux density, i.e., the charge density, was computed with the following formulas:

$$\rho = \nabla \cdot \varepsilon \mathbf{E} = \frac{\partial(\varepsilon E_x)}{\partial x} + \frac{\partial(\varepsilon E_y)}{\partial y}. \tag{28}$$

Fig. 5 shows the charge densities computed with the FDTD method, the proposed vector RBF based meshless method, and the conventional (or original) scalar RBF meshless method. We can find that the conventional RPIM does not retain the divergence-free condition. In the source-free region, numerical spurious charges are introduced as shown Fig. 5(c) and they inevitably lead to inaccurate or even totally wrong simulation results. However, the charge distribution computed with the proposed RBF meshless method is similar to that computed with the FDTD method: at the PEC fins only, we can see the charge distribution, which is expected due to the fin structure.

To further examine the divergence properties of the proposed method and the conventional RPIM, we also ran the simulations when the node distribution is not placed regularly for the finned structure (equivalent to a nonuniform situation): we slightly

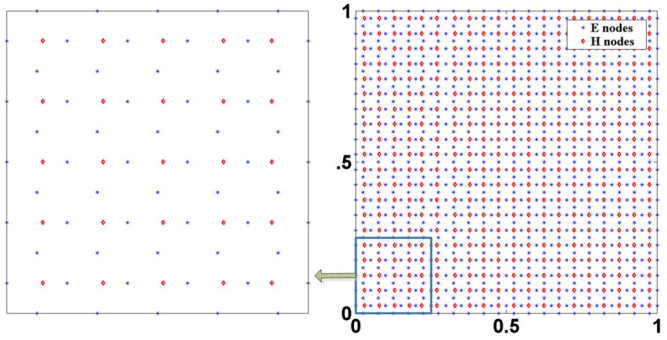

Fig. 6. Node distribution: the left side of the central axis is nonuniform and the right side is uniform.

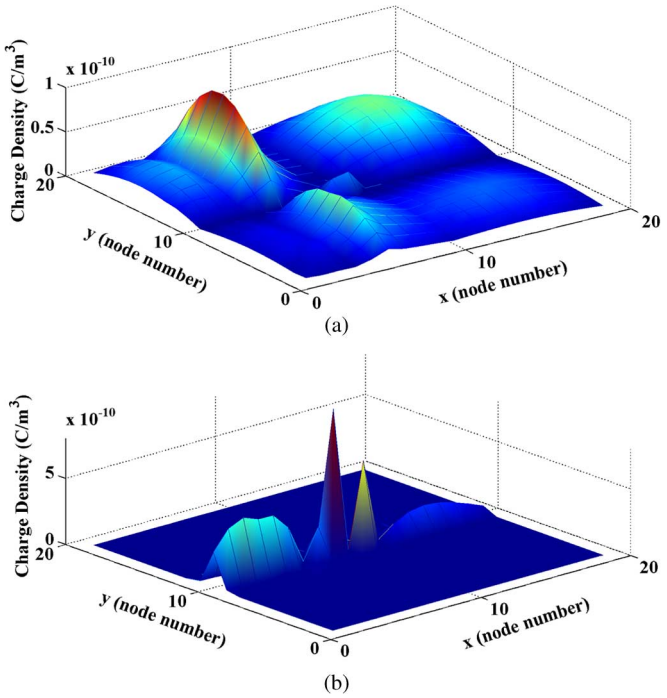

Fig. 7. Charge density distribution obtained with the: (a) conventional RPIM and (b) proposed method.

move the H-nodes off their original centers on the left side of the fin while the right side remains unchanged. The off-central displacement distance is 0.01 m and the off-central direction can be randomly chosen in the positive or negative x-axis. The node distributions are shown in Fig. 6.

The charge density obtained with the conventional RPIM and the proposed method is presented in Fig. 7. It is easy to find that the charge density obtained from the conventional RPIM does not maintain the divergence-free property in the source-free region while the proposed method does. Another interesting observation is that, in the left region, numerical spurious charge density is larger than that in the right region with the conventional RPIM. This is due to the fact that the nonuniform node distribution induces larger spurious charges as implied by (20). However, with the proposed method, spurious charges are not present. It shows that the proposed method indeed guarantees the divergence properties. In other words, numerical examples verify the theoretical analysis presented in Section III.

It should be mentioned that the above results appear not in agreement with the numerical results presented in [11] on the

stability issue. In our simulations, no monomial basis functions were used and α was chosen to be 10. They correspond to small values of $\alpha_c (= \alpha \cdot d_c^2)$, which caused unstable solutions in the cases studied in [11]. However, we did run the simulations up to 1 million iterations and no instability of our solutions was observed. We can attribute the disagreement to the fact that the Gaussian RBF, in our cases, is not directly applied to interpolate or expand the field components, but through the curl operation of (9) in order to achieve the divergence-free property. As a result, the numerical findings of [11] may not be the same as those presented in this paper as they tend to be problem dependent. Nevertheless, [11] does present valid and useful results in their cases, and we are currently investigating the stability issue and finding its solutions in an analytical way for meshelss methods in general.

VI. Conclusions

A new vector RBF based meshless method, which is theoretically proven to be divergence free, has been proposed for the transient electromagnetic analysis. Its divergence properties have been investigated and compared with those of the original scalar RBF meshless method. It has been found that the scalar RBFs cannot always retain divergence free in source-free regions while the proposed vector RBF based meshless method does. Numerical examples have been presented to verify the accuracy and divergence properties of the proposed method.

References

[1] A. Taflove, *Computational Electrodynamics: The Finite-Difference Time-Domain Method*. Norwood, MA, USA: Artech House, 1996.

[2] J.-M. Jin, *The Finite Element Method in Electromagnetics*. New York, NY, USA: Wiley, 2002.

[3] R. F. Harrington and J. L. Harrington, *Field Computation by Moment Methods*. Oxford, U.K.: Oxford Univ. Press, 1996.

[4] Z. Chen and M. M. Ney, "The method of weighted residuals: A general approach to deriving time-and frequency-domain numerical methods," *IEEE Antennas Propag. Mag.*, vol. 51, no. 1, pp. 51–70, Feb. 2009.

[5] S. Lai, B. Wang, and Y. Duan, "Meshless radial basis function method for transient electromagnetic computations," *IEEE Trans. Magn.*, vol. 44, no. 10, pp. 2288–2295, Oct. 2008.

[6] T. Kaufmann, C. Fumeaux, and R. Vahldieck, "The meshless radial point interpolation method for time-domain electromagnetics," in *IEEE MTT-S Int. Microw. Symp. Dig.*, Atlanta, GA, USA, Jun. 15–20, 2008, pp. 61–64.

[7] G. Ala, E. Francomano, A. Tortorici, E. Toscano, and F. Viola, "Smoothed particle electromagnetics: A mesh-free solver for transients," *J. Comput. Appl. Math.*, vol. 191, no. 2, pp. 194–205, Jul. 2006.

[8] D. Soares, "Time-domain electromagnetic wave propagation analysis by edge-based smoothed point interpolation methods," *J. Comput. Phys.*, vol. 234, pp. 472–486, Feb. 2013.

[9] Y. Yu and Z. Chen, "A 3-D radial point interpolation method for meshless time-domain modeling," *IEEE Trans. Microw. Theory Techn.*, vol. 57, no. 8, pp. 2015–2020, Aug. 2009.

[10] Y. Yu and Z. Chen, "Towards the development of an unconditionally stable time-domain meshless method," *IEEE Trans. Microw. Theory Techn.*, vol. 58, no. 3, pp. 578–586, Mar. 2010.

[11] T. Kaufmann, C. Engstrom, C. Fumeaux, and R. Vahldieck, "Eigenvalue analysis and longtime stability of resonant structures for the meshless radial point interpolation method in time domain," *IEEE Trans. Microw. Theory and Techn.*, vol. 58, no. 12, pp. 3399–3408, Dec. 2010.

[12] B. Jiang, J. Wu, and L. A. Povinelli, "The origin of spurious solutions in computational electromagnetics," *J. Comput. Phys.*, vol. 125, no. 1, pp. 104–123, Apr. 1996.

[13] S. Lowitzsch, "Matrix-valued radial basis functions: Stability estimates and applications," *Adv. Comput. Math.*, vol. 23, no. 3, pp. 299–315, Oct. 2005.

[14] S. Lowitzsch, "A density theorem for matrix-valued radial basis functions," *Numer. Algorithms*, vol. 39, no. 1–3, pp. 253–256, Jul. 2005.

[15] S. Lowitzsch, "Approximation and interpolation employing divergence-free radial basis functions with applications," Ph.D. dissertation, Dept. Math., Texas A&M Univ., College Station, TX, USA, 2002.

[16] C. P. McNally, "Divergence-free interpolation of vector fields from point values-exact $\nabla \cdot B = 0$ in numerical simulations," *Month. Notices Roy. Astronom. Soc., Lett.*, vol. 413, no. 1, pp. L76–L80, Mar. 2011.

[17] E. J. Kansa, "Multiquadrics—A scattered data approximation scheme with applications to computational fluid-dynamics—I surface approximations and partial derivative estimates," *Comput. Math. Appl.*, vol. 19, no. 8–9, pp. 127–145, 1990.

[18] E. J. Kansa, "Multiquadrics—A scattered data approximation scheme with applications to computational fluid-dynamics—II solutions to parabolic, hyperbolic and elliptic partial differential equations," *Comput. Math. Appl.*, vol. 19, no. 8–9, pp. 147–161, 1990.

[19] J. Wang and G. Liu, "A point interpolation meshless method based on radial basis functions," *Int. J. Numer. Methods Eng.*, vol. 54, no. 11, pp. 1623–1648, Aug. 2002.

[20] I. J. Schoenberg, "Metric spaces and completely monotone functions," *Annal. Math.*, vol. 39, no. 4, pp. 811–841, Oct. 1938.

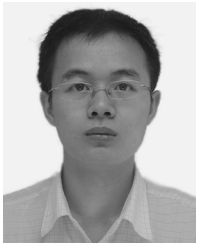

Shunchuan Yang (S'12) received the B.S. degree in optical information science and technology from Sichuan University, Sichuan, China, in 2009, the M.S. degree in optical engineering from Zhejiang University, Hangzhou, China, in 2012, and is currently working toward the Ph.D. degree at Dalhousie University, Halifax, NS, Canada.

His research interests include advanced numerical methods for computational electromagnetics (CEM) both in time and frequency domains. Those methods include the FDTD method, meshless methods, and discontinuous Galerkin FEM.

Mr. Yang was a recipient of Killam Awards of Dalhousie University.

Zhizhang (David) Chen (S'92–M'92–SM'96–F'10) received the Ph.D. degree from the University of Ottawa, Ottawa, ON, Canada.

He was a Natural Sciences and Engineering Research Council (NSERC) of Canada Post-Doctoral Fellow with the Electrical and Computer Engineering Department, McGill University, Montreal, QC, Canada. In 1993, he joined Dalhousie University, Halifax, NS, Canada, where he is currently a Professor and the Head of the Department of Electrical and Computer Engineering. He is currently on leave from Dalhousie University with the University of Electronic Science and Technology of China, Chengdu, Sichuan, China. He has authored or coauthored over 200 journal and conference papers in computational electromagnetics and RF/microwave electronics. He was one of the originators in the development of new numerical algorithms (including the unconditionally stable ADI-FDTD method) and in the design of new classes of compact RF front-end circuits for wireless communications. His current research interests include numerical time-domain modeling and simulation, RF/microwave electronics, smart antennas, and ultra-wideband and wireless transceiving technology and applications.

Dr. Chen is a Fellow of the Canadian Academy of Engineering and the Engineering Institute of Canada. He was the recipient of the 2005 Nova Scotia Engineering Award, a 2006 Dalhousie Graduate Teaching Award, the 2006 ECE Professor of the Year Award, the 2007 Faculty of Engineering Research Award of Dalhousie University, and the 2013 IEEE Canada Fessenden Medal.

Yiqiang (Johnny) Yu (M'09) received the M.Sc. degree (with distinction) in communication systems and Ph.D. degree in microwave engineering from Swansea University, Swansea, U.K., in 2003 and 2007, respectively.

Since 2011, he has been an Associate Professor with East China Jiaotong University, Nan Chang, Jiang Xi, China. He is also an Adjunct Professor and Senior Research Engineer with the Department of Electrical and Computer Engineering, Dalhousie University, Halifax, NS, Canada. His primary interest is in applications of computational electromagnetics, particularly the use of finite-difference methods, MOM, and meshless methods in both the time and frequency domains. His interests also include RF/microwave components design, antennas design and measurement, electromagnetic interference (EMI)/electromagnetic compatibility (EMC) analysis and design, and iterative solvers and preconditioning techniques for large-scale matrix computation.

Prof. Yu was a recipient of the Overseas Research Fund from United Kingdom Overseas Research Award Program (2004–2007). He was also a recipient of the National Natural Science Foundation of China Science Research Fund (2011–2013).

Sergey Ponomarenko received the Five-Year Diploma in physics from Novosibirsk State University, Novosibirsk, Russia, in 1994, and the Ph.D. degree in theoretical optical physics from the University of Rochester, Rochester NY, USA, in 2002.

His work toward the Ph.D. degree and his later research as a Postdoctoral Associate (2002–2004) was supervised by Emil Wolf, a pioneer of optical coherence theory. In 2004, he accepted a Director's Postdoctoral Fellowship with Los Alamos National Laboratory, where, until July 2006, he was a Director's Postdoctoral Fellow. In July 2006, he joined the Faculty of the Department of Electrical and Computer Engineering, Dalhousie University, Halifax, NS, Canada, as a Canada Research Chair. He renewed his Canada Research Chair appointment in 2011. He is currently an Associate Professor with Dalhousie University. He has authored or coauthored over 55 scientific papers in leading peer-reviewed journals. His research interests fall into the general areas of optical physics, photonics, and electromagnetics.